

# Formation and evolution of dwarf elliptical galaxies

## I. Structural and kinematical properties

S. De Rijcke<sup>1, \*</sup>, D. Michielsen<sup>1</sup>, H. Dejonghe<sup>1</sup>, W. W. Zeilinger<sup>2</sup>, and G. K. T. Hau<sup>3</sup>

<sup>1</sup> Sterrenkundig Observatorium, Ghent University, Krijgslaan 281, S9, B-9000 Gent, Belgium,  
e-mail: sven.derijcke@UGent.be

<sup>2</sup> Institut für Astronomie, Universität Wien, Türkenschanzstraße 17, A-1180 Wien, Austria

<sup>3</sup> Department of Physics, South Road, Durham, DH1 3LE, UK

Received September 15, 1996; accepted March 16, 1997

**Abstract.** This paper is the first in a series in which we present the results of an ESO Large Program on the kinematics and internal dynamics of dwarf elliptical galaxies (dEs). We obtained deep major and minor axis spectra of 15 dEs and broad-band imaging of 22 dEs. Here, we investigate the relations between the parameters that quantify the structure (B-band luminosity  $L_B$ , half-light radius  $R_e$ , and mean surface brightness within the half-light radius  $I_e = L_B/2\pi R_e^2$ ) and internal dynamics (velocity dispersion  $\sigma$ ) of dEs. We confront predictions of the currently popular theories for dE formation and evolution with the observed position of dEs in  $\log L_B$  vs.  $\log \sigma$ ,  $\log L_B$  vs.  $\log R_e$ ,  $\log L_B$  vs.  $\log I_e$ , and  $\log R_e$  vs.  $\log I_e$  diagrams and in the  $(\log \sigma, \log R_e, \log I_e)$  parameter space in which bright and intermediate-luminosity elliptical galaxies and bulges of spirals define a Fundamental Plane (FP). In order to achieve statistical significance and to cover a parameter interval that is large enough for reliable inferences to be made, we merge the data set presented in this paper with two other recently published, equally large data sets.

We show that the dE sequences in the various univariate diagrams are disjunct from those traced by bright and intermediate-luminosity elliptical galaxies and bulges of spirals. It appears that semi-analytical models (SAMs) that incorporate quiescent star formation with an essentially  $z$ -independent star-formation efficiency, combined with post-merger starbursts and the dynamical response after supernova-driven gas-loss, are able to reproduce the position of the dEs in the various univariate diagrams. SAMs with star-formation efficiencies that rise as a function of redshift are excluded since they leave the observed sequences traced by dEs virtually unpopulated. dEs tend to lie above the FP and the FP residual declines as a function of luminosity. Again, models that take into account the response after supernova-driven mass-loss correctly predict the position of dEs in the  $(\log \sigma, \log R_e, \log I_e)$  parameter space as well as the trend of the FP residual as a function of luminosity.

While these findings are clearly a success for the hierarchical-merging picture of galaxy formation, they do not necessarily invalidate the alternative “harassment” scenario, which posits that dEs stem from perturbed and stripped late-type disk galaxies that entered clusters and groups of galaxies about 5 Gyr ago.

**Key words.** Galaxies: dwarf – Galaxies: fundamental parameters – Galaxies: kinematics and dynamics – Galaxies: evolution – Galaxies: formation

### 1. Introduction

It is known for almost two decades now that dynamically hot galaxies (elliptical galaxies and bulges of spiral galaxies) are not scattered randomly in the three-dimensional space spanned by B-band luminosity ( $\log L_B$ , expressed in solar B-band luminosities), half-light radius ( $\log R_e$ , expressed in kiloparsecs), and velocity dispersion ( $\log \sigma$ , expressed in  $\text{km s}^{-1}$ ) but that instead they occupy a slender plane: the Fundamental Plane (FP) (Djorgovski & Davis (1987), Dressler *et al.* (1987), Bender *et al.* (1992)). Projections of the FP onto the coor-

dinate planes, in combination with the particular way in which galaxies are distributed within the FP, produce the univariate relations between luminosity and velocity dispersion ( $\log L_B = \text{const.} + 3.739 \log \sigma$ , Faber & Jackson (1976)), luminosity and half-light radius ( $\log L_B = \text{const.} + 1.187 \log R_e$ , Fish (1963)), surface brightness (expressed in solar B-band luminosities per square parsec) and half-light radius ( $\log I_e = \text{const.} - 0.813 \log R_e$ , Kormendy (1977)), and luminosity and surface brightness ( $\log L_B = \text{const.} - 1.460 \log I_e$ , Binggeli *et al.* (1984)) (see Guzmán *et al.* (1993) for a compilation of these so-called fundamental relations).

Dwarf elliptical galaxies (dEs) are small, low-luminosity galaxies ( $M_B \gtrsim -18$  mag) (Ferguson & Binggeli (1994)). They are among the most numerous galaxy species in the

Send offprint requests to: S. De Rijcke

\* Postdoctoral Fellow of the Fund for Scientific Research - Flanders (Belgium)(F.W.O.)

universe and are found abundantly in groups and clusters of galaxies. Their diffuse, approximately exponentially declining surface-brightness profiles set them apart from the compact ellipticals (cEs) which, while occupying the same luminosity range as the dEs, have much higher central surface brightnesses and a de Vaucouleurs-like surface-brightness profile. We distinguish dwarf lenticular galaxies (dS0s) from dEs by their highly flattened appearance (E6/E7) and their disk-like isophotes. The locus of the dEs and dS0s in the  $(\log \sigma, \log R_e, \log I_e)$  space and in the univariate diagrams that require kinematical information (such as the Faber-Jackson relation, hereafter FJR) was up to now rather uncertain. After the early work by Nieto *et al.* (1990), Bender *et al.* (1992), and Guzmán *et al.* (1993), relatively little attention has been paid to the relations between the internal kinematics and the structural parameters of these faint, small elliptical galaxies and, particularly, to what we can learn from such relations regarding the origin and evolution of dEs. This is in part due to their low surface brightness, which makes spectroscopy, required for the extraction of stellar kinematics, very time-consuming. This also limits the size of the individual data sets and consequently compromises the statistical significance of the results. Still, explaining the scaling relations among the structural parameters of dwarf galaxies, which are believed to be the building blocks of more massive galaxies, is a crucial test for theories of cosmological structure formation. A comparison of theoretical predictions with observations can put strong constraints on the cosmological star-formation history and help to refine prescriptions for e.g. star formation and energy feedback from supernova explosions (which play a crucial role in low-mass dwarf galaxies).

This paper is the first in a series in which we present the results based on the kinematics of a sample of 15 dEs and dS0s and photometry of 22 dEs/dS0s, both in group and cluster environments, observed in the course of an ESO Large Program. We explore the relations between the various structural parameters of dEs and compare them with theoretical predictions. This paper is organised as follows: we briefly discuss the observations and data reduction procedures in section 2. In section 3, the theoretical models with which we compare our data are presented. The univariate relations between the different structural parameters are discussed in section 4. The position of the dEs with respect to the Fundamental Plane is presented in section 5. We end with a discussion of the results in section 6.

## 2. Observations and data reduction

Within the framework of an ESO Large Program, we observed deep major and minor axis spectra with unprecedented spatial and spectral resolution of a sample of 15 dEs and dS0s, both in group (NGC5044, NGC5898, and NGC3258 groups) and cluster environments (Fornax cluster). We also collected Bessel VRI-band images of 22 dEs and dS0s (including the 15 dEs/dS0s of the spectroscopic sample). The targets were selected because they were faint galaxies with elliptical isophotes (with absolute magnitudes in the range  $-13.3 \geq M_B \geq -18$  mag in order to distinguish them from the brighter ellipticals and the fainter dwarf spheroidals (dSphs))

and had a high enough surface brightness ( $\mu_{e,B} \leq 23.5$  mag, with  $\mu_{e,B}$  the mean B-band surface brightness within the half-light radius) to make the extraction of reliable kinematics out to roughly  $1.5 - 2 R_e$  feasible. In order to obtain a good spatial sampling of the kinematics, the seeing FWHM should be much smaller than a galaxy's half-light radius so galaxies with a half-light radius smaller than  $R_e \approx 4''$  were rejected as possible targets. There was no direct kinematical selection criterion.

The data were obtained with the FORS2 imaging spectrograph mounted on the unit telescopes Kueyen and Yepun of the VLT. The images were bias-subtracted and flatfielded using skyflats taken during twilight of the same night as the science frames. The sky background was removed by fitting a tilted plane to regions of the images free of stars or other objects and subtracting it. The photometric zeropoints in each band were measured using photometric standard stars observed during the same night as the science frames. The images were corrected for airmass and for interstellar extinction, using the Galactic extinction estimates from Schlegel *et al.* (1998). We measured the surface-brightness profile, position angle, and ellipticity as a function of the geometric mean of major and minor axis distance, denoted by  $a$  and  $b$  respectively, using our own software. Basically, the code fits an ellipse through a set of positions where a given surface brightness level is reached (cosmics, hot pixels, and foreground stars were masked and not used in the fit). The shape of an isophote, relative to the best fitting ellipse, is quantified by expanding the intensity variation along this ellipse in a fourth order Fourier series with coefficients  $S_4$ ,  $S_3$ ,  $C_4$  and  $C_3$ :

$$I(a, \theta) = I_0(a) [1 + C_3(a) \cos(3\theta) + C_4(a) \cos(4\theta) + S_3(a) \sin(3\theta) + S_4(a) \sin(4\theta)]. \quad (1)$$

Here,  $I_0(a)$  is the average intensity of an isophote with semi-major axis  $a$  and the angle  $\theta$  is measured from the major axis. The basic photometric parameters of the galaxies are presented in Table 1. This smooth representation of a galaxy's surface-brightness profile,  $I(a, \theta)$ , was integrated over circular apertures out to the last isophote we could reliably measure in order to calculate its total magnitude. We did not wish to extrapolate the surface brightness profile or the growth curve beyond the region covered by the data (e.g. by using a Sérsic profile) because of the uncertainties inherent to this procedure. However, our images go down at least 8 mags. Cutting off an exponential surface brightness profile 8 mags below its central value results in an underestimate of the total luminosity by less than one percent (a cut-off at 6 mags below the central surface brightness, as in a few less deep images, results in an underestimate of the total luminosity by about 2.5% for an exponential profile).

The spectra, with typical exposure times of 5–8 h per position angle and a seeing in the range  $0.3'' - 1.0''$  FWHM, cover the wavelength region around the strong CaII triplet absorption lines ( $\sim 8600 \text{ \AA}$ ). All standard data reduction procedures (bias-subtraction, flatfielding, cosmic removal, wavelength-calibration, sky-subtraction, flux-calibration) were carried out

**Table 1.** Structural properties of the observed dEs. The FCC dEs are members of the Fornax Cluster (Ferguson (1989)); the FS dEs belong to the NGC5044 and NGC3258 groups and are cataloged by Ferguson & Sandage (1990). NGC5898\_DW1 and NGC5898\_DW2 are two previously uncataloged dEs in the NGC5898 group (where DW stands for DWARF). For each galaxy, the equatorial coordinates, the B-band apparent magnitude  $m_B$  (taken from Ferguson (1989) and Ferguson & Sandage (1990), except for FCC046 and FCC207 for which we have obtained B-band images), the luminosity-weighted ellipticity  $\epsilon = 1 - q$ , with  $q$  the isophotal axis ratio, outside the inner 1 arcsec where the ellipticity measurement is affected by seeing, the luminosity-weighted velocity dispersion  $\sigma$  (km s $^{-1}$ , see eq. (2) for a precise definition of  $\sigma$ ), the half-light radius  $R_e$  (arcsec, this is the radius of the circular aperture that encloses half of the light), derived from the R-band images, and the B-band mean surface brightness within one half-light radius  $\mu_{e,B}$  are listed. We used our R-band  $R_e$  to calculate  $\mu_{e,B}$ . This does not influence our results in any way since we found  $R_e$  not to differ between R, B, and V-band images. For 7 dEs, only photometry is available.

name	$\alpha$ (J2000)	$\delta$ (J2000)	$m_B$	$\epsilon$	$\sigma$	$R_e$	$\mu_{e,B}$
FCC043	03 26 02.2	-32 53 40	13.91	0.26	56.4 $\pm$ 3.7	16.9	22.05
FCC046	03 26 25.0	-37 07 41	15.99	0.36	61.4 $\pm$ 5.0	6.7	22.12
FCC100	03 31 47.6	-35 03 07	15.30	0.28	/	11.7	22.63
FCC136	03 34 29.5	-35 32 47	14.81	0.21	64.3 $\pm$ 3.8	14.2	22.57
FCC150	03 35 24.1	-36 21 50	15.70	0.19	63.8 $\pm$ 3.9	5.7	21.48
FCC188	03 37 04.5	-35 35 26	16.10	0.06	/	9.3	22.94
FCC204	03 38 13.6	-33 07 38	14.76	0.61	67.2 $\pm$ 4.4	11.5	22.06
FCC207	03 38 19.3	-35 07 45	16.19	0.15	60.9 $\pm$ 6.6	8.4	22.81
FCC245	03 40 33.9	-35 01 23	16.00	0.11	39.5 $\pm$ 4.2	11.4	23.28
FCC252	03 40 50.4	-35 44 54	16.00	0.08	/	7.9	22.47
FCC266	03 41 41.4	-35 10 12	15.90	0.11	42.4 $\pm$ 3.4	7.1	22.15
FCC288	03 43 22.6	-33 56 25	15.10	0.72	48.5 $\pm$ 3.3	9.5	21.99
FCC303	03 45 14.1	-36 56 12	15.50	0.09	/	11.6	22.81
FCC316	03 47 01.4	-36 26 15	16.30	0.26	/	9.0	23.06
FCC318	03 47 08.2	-36 19 36	16.10	0.18	/	10.6	23.22
FS029	13 13 56.2	-16 16 24	15.70	0.54	59.6 $\pm$ 3.6	8.9	22.44
FS075	13 15 04.1	-16 23 40	16.87	0.10	/	6.8	23.03
FS076	13 15 05.9	-16 20 51	16.10	0.07	56.8 $\pm$ 3.8	4.4	21.41
FS131	13 16 49.0	-16 19 42	15.30	0.54	87.0 $\pm$ 3.2	8.1	21.83
FS373	10 37 22.9	-35 21 37	15.60	0.23	73.1 $\pm$ 3.1	7.9	22.03
NGC5898_DW1	15 18 13.0	-24 11 47	15.66	0.34	43.5 $\pm$ 3.0	8.7	22.35
NGC5898_DW2	15 18 44.7	-24 10 51	16.10	0.57	44.2 $\pm$ 3.4	5.9	21.95

with ESO-MIDAS<sup>1</sup>, IRAF<sup>2</sup>, and our own software. We fitted the dispersion relation with a cubic spline, which rectified the lines of the arc spectra to an accuracy of 1 – 2 km s $^{-1}$  FWHM. We extracted the stellar kinematical information by fitting a weighted mix of late G to late K giant stars, broadened with a parameterised line-of-sight velocity distribution (LOSVD) to the galaxy spectra. We approximated the LOSVD by a fourth-order Gauss-Hermite series (Gerhard (1993), van der Marel & Franx (1993)) (the kinematics of the full sample and a complete discussion of the data acquisition and analysis will be presented in the next paper in this series, De Rijcke *et al.*, in prep.). The strong CaII lines, which contain most of the kinematical information, are rather insensitive to the age and metallicity of an old stellar population (see e.g. Michielsen *et al.* (2003), Falcón-Barroso *et al.* (2003), Saglia *et al.* (2002)), so template

<sup>1</sup> ESO-MIDAS is developed and maintained by the European Southern Observatory

<sup>2</sup> IRAF is distributed by the National Optical Astronomy Observatories, which are operated by the Association of Universities for Research in Astronomy, Inc., under cooperative agreement with the National Science Foundation.

mismatch does not significantly affect our results. The spectra contain useful kinematical information out to 1.5–2  $R_e$ .

### 3. Theoretical models for dE formation

Here, we discuss the models for dE formation and evolution which in the following sections will be compared with the data. First, three different calculations are introduced that are all based on the idea that dEs are primordial objects that lost their gas in a supernova-driven galactic wind (a.k.a. the “wind model”) and second, we discuss model predictions based on the harassment scenario.

#### 3.1. The “wind model”

The first detailed models of the evolution of galaxies taking into account the dynamical response after a supernova-driven galactic wind (hence the name of this class of models) were presented by Yoshii & Arimoto (1987) (hereafter YA87). These models follow the evolution of stellar systems using one-zone models without internal structure and with masses between  $10^5 M_\odot$  and  $2 \times 10^{12} M_\odot$ . They assume an empirical scaling law between the gravitational binding energy  $\Omega$  and total mass

$M: \Omega \propto M^{1.45}$  (Fish (1964), Saito (1979)). This translates into a mass-gravitational radius relation of the form  $R_G \propto M^2/\Omega \propto M^{0.55}$ , a mass-density relation  $\rho \propto M/R^3 \propto M^{-0.65}$ , and a velocity dispersion-mass relation  $\sigma \propto \sqrt{\Omega/M} \propto M^{0.225}$  before any mass-loss has occurred. The star-formation timescale  $t_{\text{SF}}$  is proportional to the minimum of the collision time of molecular clouds and the free-fall time of individual clouds. In both cases,  $t_{\text{SF}} \propto 1/\sqrt{\rho}$  with the proportionality constant chosen such that the present-day color-magnitude relation, from giant ellipticals down to globular clusters, is reproduced. The structure of these models is altered as they expand in response to the loss of a mass-fraction  $f$  in the form of supernova-driven galactic winds. The value of  $f$  is determined by the timing of the galactic winds, with later winds expelling a smaller gas fraction than earlier ones. In these models, the time-scales on which all physical processes operate are determined by  $M$ , making  $f$  also a function of  $M$ . The crux is, of course, for  $f$  to have the correct behaviour as a function of  $M$  in order to reproduce the observed relations between the different structural parameters of spheroidal galaxies. Since  $R_G$  is roughly proportional to  $R_e$  in a constant- $M/L$  model, and the precise value of the radius does not affect the physics of the models anyway, we scaled the mass-radius relation such that the present-day half-light radii of ellipticals with a luminosity  $\log L_B = 10.4$  ( $M_B = -20.5$  mag) are reproduced. This is the boundary between, roughly speaking, the disk, cuspy, isotropic intermediate-brightness ellipticals and the boxy, anisotropic bright ellipticals with a core (Bender *et al.* (1989), Graham & Guzmán (2003)).

More recent semi-analytical models (SAMs) (Somerville *et al.* (2001), Nagashima & Yoshii (2004)) take into account the hierarchical merger tree that leads up to the formation of a galaxy of a given mass in a  $\Lambda$ CDM cosmology ( $\Omega_{\text{baryon}} \approx 0.02$ ,  $\Omega_{\text{matter}} = 0.3$ ,  $\Omega_\Lambda = 0.7$ ,  $H_0 = 70 \text{ km s}^{-1} \text{ Mpc}^{-1}$ ). SAMs make use of prescriptions for star-formation, energy feedback from supernova explosions, gas cooling, tidal stripping, dust extinction, and the dynamical response to starburst-induced gas ejection and, despite the inevitable oversimplifications in the description of immensely complex processes such as star formation, they are able to account pretty well for many observed properties of galaxies. E.g., Somerville *et al.* (2001) compare their SAMs with the comoving number density of galaxies, the evolution of the galaxy luminosity function and the H $\alpha$  content of the universe as a function of redshift, and the star-formation history of the universe (the “Madau diagram”). Based on this comparison, these authors favor the idea that merger-induced star bursts have played an important role in enhancing the star-formation efficiency at high redshift. Nagashima & Yoshii (2004) (NY04) moreover take into account the gas ejection and the ensuing dynamical response of a galaxy after a merger-induced star-burst. These authors compare the galaxies formed in their SAMs with the observed properties of dynamically hot galaxies (from the faint Local Group dSphs up to the very brightest elliptical galaxies) and come to roughly the same conclusions as Somerville *et al.* (2001). Despite their simplicity, the YA87 models already capture a lot of the physics of galaxy formation, at least in the mass-regime of the dEs, which apparently formed while their progenitors were

still largely gaseous. *In all figures, we will use them as an instructive proxy for the physically more motivated SAMs of e.g. Somerville *et al.* (2001) and Nagashima & Yoshii (2004).* Using the tables given in Yoshii & Arimoto (1987), we fitted cubic splines to all relevant parameters as functions of  $M$  in order to be able to plot them as continuous sequences in the figures in the following sections.

In Chiosi & Carraro (2002) (hereafter CC02), the evolution of spherical elliptical galaxies in a standard CDM universe ( $\Omega_{\text{baryon}} = 0.1$ ,  $\Omega_{\text{dark}} = 0.9$ ,  $\Omega_\Lambda = 0$ ) is followed using N-body/SPH simulations with prescriptions for star-formation, feedback, cooling, and chemical evolution. A protogalaxy is assumed to virialize at a redshift  $z = 5$ , when it had an over-density  $1 + \delta \sim 200$ , after which star-formation ensues. Two series of models, with masses between  $10^8$  and  $10^{13} M_\odot$  and with different initial densities, are presented. Models of series A have a high initial density (they virialized at redshift  $z = 5$ , when the universe was still very dense), models of series B have low initial densities (they virialized at much lower redshift). These models allow for a more realistic description of the galactic wind as compared to YA87: only gas particles with velocities above the local escape speed are blown away. This reduces the amount of mass that is lost and leads to a much milder structural evolution compared to the YA87 models. Contrary to the YA87 models, dwarf galaxies are found to have the longest star formation histories. Massive ellipticals hold on very strongly to their gas reservoirs, allowing the gas to be converted almost completely into stars in a single burst. In dwarf galaxies, on the other hand, supernova explosions disperse the gas, switching off further star formation. Gas cools, sinks back in and the star-formation efficiency goes up again after which subsequent supernova explosions disperse the gas and so on. This gives rise to very inefficient, oscillating but long-lived star formation. As aforementioned, the way star formation is implemented in the YA87 models causes the star-formation efficiency to be highest in low-mass galaxies, they simply do not continue forming stars for very long. By the time a galactic wind sets off, most of the gas has been converted into stars. Very massive galaxies form stars most slowly but they hang onto their gas very strongly, leaving enough time for most of the gas to be converted into stars. Hence, galaxies around  $\log(L_B) = 7$  ( $M_B = -12$  mag) experience the most drastic mass-loss while more and less luminous galaxies are less affected by gas ejection. This effect is most likely due to the extreme simplicity of the models. The more complex models, with more realistic star-formation histories, do not show this behaviour.

Both the YA87 and CC02 models do not take into account mergers. As a consequence, they will underestimate the velocity dispersions and half-light radii and overestimate the surface brightnesses of massive ellipticals (see e.g. Hernquist (1992) and Dantas *et al.* (2003) for the effects of dissipationless mergers and Hernquist *et al.* (1993) and Bekki (1998) for merger simulations taking into account the presence of gas). SAMs (e.g. NY04) follow the merger tree leading up to a galaxy (including dissipationless mergers) and hence do a much better job at reproducing the characteristics of massive galaxies. Hence, the failure of the YA87 and CC02 models for bright galaxies does not signal a problem with CDM. These models

simply lack the physics necessary to explain the properties of bright ellipticals.

The N-body/SPH models presented by Kawata (1999) and Kawata (2001) (K01) are based roughly on the same premises as those of CC02, although the details differ. Using an N-body/SPH code, the evolution of a slowly rotating (spin parameter  $\lambda = 0.02$ ) region in a standard CDM universe, on which small-scale density fluctuations are laid out, is followed from  $z = 40$  up to the present. Overdense clumps within this region collapse, merge, and finally form a single elliptical galaxy. Regions with masses between  $10^{11}$  and  $8 \times 10^{12} M_{\odot}$  are modeled. E.g., for a region with a total mass  $M = 8 \times 10^{11} M_{\odot}$ , star formation starts in merging clumps at  $z \approx 3.5$  and the final galaxy is in place at  $z \approx 1.9$ . No merging takes place after  $z \approx 0.8$ . The influence of the energy feedback efficiency of supernova explosions (SNII and SNIA) on the evolution of elliptical galaxies and bright dEs is explored. The more efficient the supernovae inject kinetic energy into the interstellar medium, the sooner the gas is blown away. This results in more expelled gas and more structural evolution in low-mass galaxies. Two series of models are calculated: a series with very efficient kinetic feedback, which is able to reproduce the observed color-magnitude relation of elliptical galaxies, and one with minimal feedback. As an example: a bright dwarf galaxy with an initial total mass  $M = 10^{11} M_{\odot}$  and with a high feedback efficiency develops a galactic wind at  $z \approx 1.7$ . By  $z \approx 1.2$ , most of the gas has been blown out. For these models, only photometric quantities are calculated.

It should be noted that CC02 and K01 use a CDM cosmology whereas NY04 use  $\Lambda$ CDM. This is probably not a major concern. CC02 follow the evolution of an isolated galaxy, disconnected from the universal expansion. The only cosmological parameter that goes into these calculations is the density of the universe at the virialization redshift of the galaxy. However, at  $z \sim 5$ , a CDM universe very much resembles a  $\Lambda$ CDM universe since  $\Omega_{\Lambda}$  started to dominate  $\Omega_{\text{matter}}$  only at  $z \sim 0.3$ . In K01, most of the merging activity, which is influenced by the dynamics of the universe, has ended around  $z = 2$ . So, hierarchical merging takes place at a cosmic time when CDM and  $\Lambda$ CDM universes do not differ much. The YA87 models, due to their simplicity, are essentially devoid of cosmological considerations. Moreover, slight effects due to cosmology can probably be offset by using slightly different star-formation or feedback efficiencies. This makes us confident that the different cosmologies do not yield significantly different predictions for the properties of individual galaxies.

### 3.2. The harassment scenario

Alternatively, dEs could stem from late-type disk galaxies that entered the clusters and groups of galaxies about 5 Gyr ago ( $z \sim 0.5$ ). *N*-body simulations show that gravitational interactions trigger bar-formation in any small late-type disk galaxy (Scd-Irr) orbiting in a cluster (Moore *et al.* (1996), Moore *et al.* (1998)) or around a massive galaxy in a group environment (Mayer *et al.* (2001)) and strip large amounts of stars, gas, and dark matter from it by tidal forces.

Internal dynamical processes (such as the buckling of the bar) subsequently transform a disk galaxy into a dynamically hot spheroidal dE within a timespan of a few Gyr (Mastropietro *et al.* (2004)). Gas (if it is not stripped off by the ram pressure of the intergalactic medium, see e.g. Marcolini *et al.* (2003)) is funneled inwards by the non-axisymmetric force field of the bar (Mayer *et al.* (2001)). If this gas is converted into stars, the resulting galaxy is likely to have a higher central surface brightness than its progenitor and would probably resemble a nucleated dE. Purely stellar dynamical processes such as bar formation and buckling lead to a more shallow central density enhancement. The dEs formed in these simulations rotate quite rapidly and some still display some memory of their former state. Examples are dEs with embedded stellar disks (Barazza *et al.* (2002), De Rijcke *et al.* (2003a), Graham *et al.* (2003)) or kinematically decoupled cores (De Rijcke *et al.* (2004)). This model explicitly takes into account the fact that dEs are found predominantly in clusters and groups of galaxies. It also offers a natural explanation for the Butcher-Oemler effect (Butcher & Oemler (1978)): at  $z \sim 0.4$ , a population of blue, distorted galaxies is present in clusters of galaxies while no such objects reside in present-day clusters. The former could be late-type galaxies caught in the predicament of being harassed and transformed into more spheroidal objects.

Clearly, the parameter space that should be explored to make firm predictions based on this scenario is huge. One should start with gas-rich late-type galaxies of various masses and with different scale-lengths, placed on different orbits in a variety of cluster and group environments, using realistic prescriptions for star-formation, energy feedback, gas cooling, and ram-pressure stripping by the intra-cluster medium. As long as this formidable task has not been performed, we will have to settle with what can be gleaned from the few calculations that have been published up to now. These show that, harassment being a stochastic process whose effects depend in a very complicated way on the orbit of a progenitor galaxy through a cluster, it is rather unlikely that dEs end up close to a slender plane like the FP. The half-light radius of a dE formed through harassment is about half that of its progenitor, with the central surface brightness about two to three times higher than the original value (Mayer *et al.* (2001)). The velocity dispersion has also roughly doubled. Moreover, it is very likely that interactions induce star-bursts and hence that dEs formed through harassment harbor stellar populations of different ages, further adding to the expected scatter about the FP (Forbes, Ponman, Brown (1998)). Although more simulations are needed to converge on a coherent picture of the effects of harassment, two predictions can already be made: (1) some dEs should still contain some memory of their disk, gaseous past and (2) only weak correlations with large scatter are expected between structural parameters. The latter is due to the stochastic nature of harassment and, if the Butcher-Oemler galaxies at  $z \sim 0.4$  are anything like the present-day Scd-Irr galaxies, due to the large scatter of the progenitor galaxies in the FP (Burstein *et al.* (1997)).

Yet another possible way to produce dwarf galaxies is described by Kroupa (1998) or Duc *et al.* (2004). The hundreds

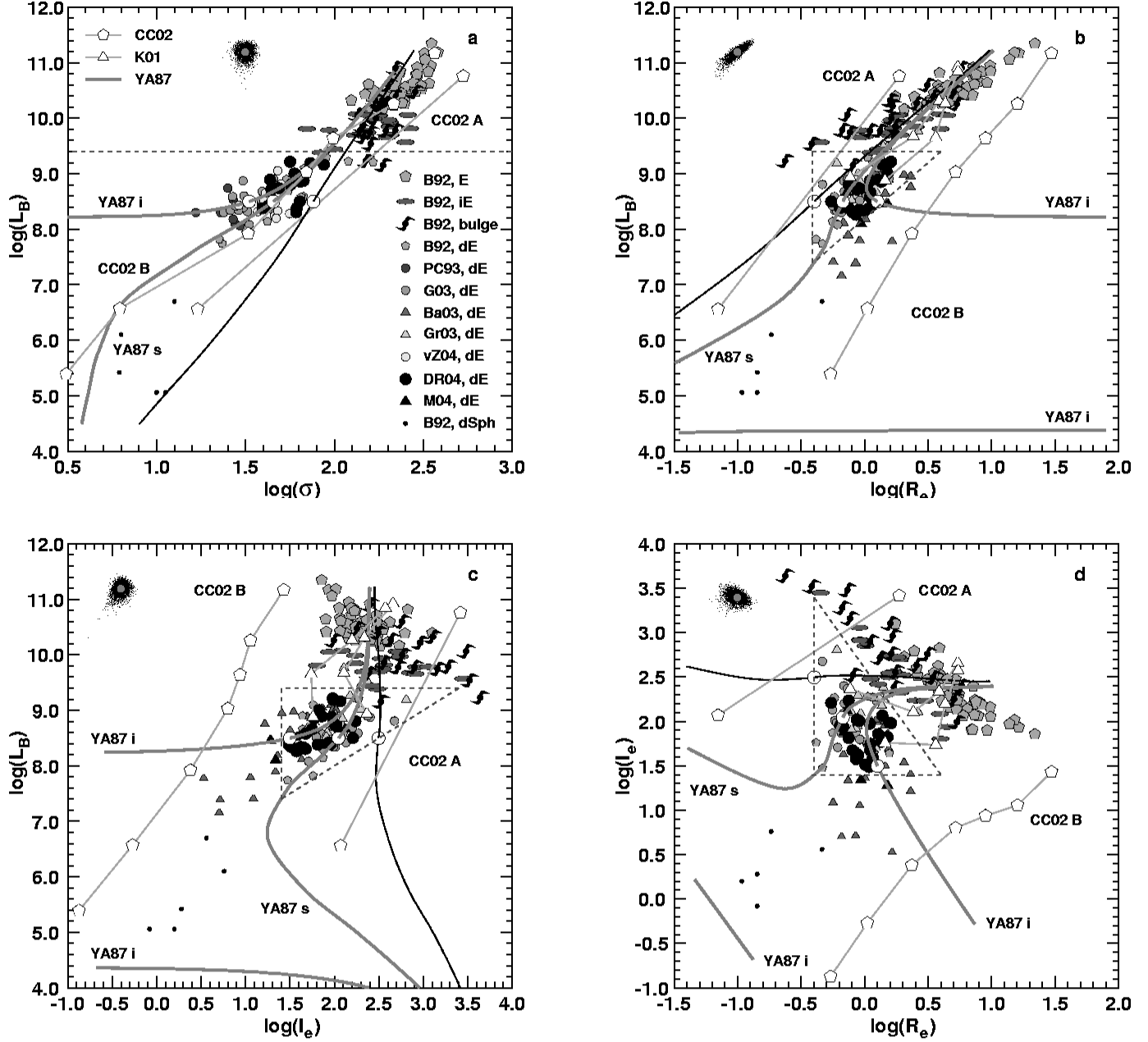


**Fig. 1.** Panel **a**: the  $\sigma - L_B$  relation; panel **b**: the  $R_e - L_B$  relation; panel **c**: the  $I_e - L_B$  relation; panel **d**: the  $R_e - I_e$  relation. The regions in these diagrams that satisfy our selection criteria are delineated by dotted lines.  $L_B$  is expressed in solar B-band luminosities,  $\sigma$  in  $\text{km s}^{-1}$ ,  $R_e$  in kiloparsecs, and  $I_e$  in solar B-band luminosities per square parsec. The symbols representing the various datasets, galaxy types (bright ellipticals: E, intermediate-luminosity ellipticals: iE, bulges of spiral galaxies: bulge, dwarf ellipticals: dE, dwarf spheroidals: dSph), and theoretical models are indicated in panel **a**. The black line traces the zero mass-loss relation of the YA87 models. The thick grey lines trace the relations after slow (YA87 s) or instantaneous (YA87 i) gas removal. The position of a typical dE with apparent magnitude  $m_B = 16$  at the distance of Fornax before and after supernova-driven mass-loss is indicated with white circles. The CC02 models (white pentagons) of series A (CC02 A) collapse to a final state with a very small half-light radius and a large velocity dispersion. The models of series B (CC02 B) on the other hand reproduce the observed  $\sigma - L_B$  relation but have half-light radii that are too large. On the whole, the CC02 models are able to reproduce the observed slopes of the several structural relations. The photometric properties of the K01 models (white triangles) roughly agree with the observations and the YA87 models. For a given mass, the trend for K01 models as a function of feedback efficiency parallels that of the YA87 models as a function of mass-loss timescale. In the upper left corner of each panel, a cloud of 3000 simulated data points gives an idea of the systematic and statistical uncertainty on a typical DR04 data point (indicated by a grey dot).

of young compact massive star clusters formed during the merger of two gaseous disk galaxies may coalesce within a few 100 Myr to form a small number of objects, with masses of order  $10^9 M_\odot$ , with negligible dark-matter content, and with a half-mass radius of a few 100 pc. However, simulations have thus far not been able to make predictions for the present-day properties of these so-called tidal dwarf galaxies. Also, major mergers cannot have produced a significant fraction of the dE population since each merger only yields one or two tidal dwarf galaxies. For these reasons, and since the objects formed this way are less massive than the dEs considered here and in many respects are more like the Local Group dSphs, we will not discuss this formation mechanism here.

#### 4. Univariate relations

In the following, we confront the predictions of the models discussed in section 3, with the observed relations between the structural and kinematical parameters of dynamically hot galaxies. The most massive representatives of this family of galaxies are the giant ellipticals (B-band luminosity  $\log L_B \sim 11.5$  ( $M_B = -23.3$  mag)); the least massive systems are the Local Group dwarf spheroidals ( $\log L_B \sim 6$  ( $M_B = -9.5$  mag)). Three data sets of kinematics of dEs in the luminosity range  $\log L_B \approx 8 - 9.2$  ( $M_B = -14.5$  to  $-17.4$ ) are currently available: our sample of 15 group and cluster dEs/dS0s (DR04), the sample of 17 Virgo cluster dEs observed by Geha *et al.* (2003) (G03) and the 16 Virgo cluster dEs from van Zee *et al.*, 2004 (vZ04) (which has an overlap of 5 objects with the G03 sample). Since none of the three datasets on its own can boast statistical significance or cover a parameter interval large enough for reliable inferences to be made, it is natural to combine them, bringing the total number of dEs with spatially resolved kinematics to 43. For completeness, we also compare our results with the central velocity dispersions of nucleated dEs measured by Peterson & Caldwell (1993) (PC93).

In diagrams relating only photometrical parameters, we have included the sample of 25 Virgo cluster dEs and dS0s of Barazza *et al.* (2003) (Ba03), which was used for the determination of surface-brightness fluctuation (SBF) distances, the Fornax dEs presented in Michielsen *et al.* (2004) (M04), and the 18 Coma dEs analysed in Graham & Guzmán (2003) (Gr03). The dwarf galaxies in the Ba03 sample were selected because they have large half-light radii and yield as many independent SBF measurements as possible. Hence, the Ba03 sample traces the dE sequences in the photometric univariate diagrams in regions as yet unexplored by spectroscopic samples. The relevant data for giant ellipticals, intermediate-luminosity ellipticals, bulges, dwarf spheroidals and a handful of dEs come from Bender *et al.* (1992) (B92). Where necessary, all datasets have been converted to B-band luminosities assuming  $B - V = 0.7$  and to a Hubble parameter  $H_0 = 70 \text{ km s}^{-1} \text{ Mpc}^{-1}$  (Freedman *et al.* (2001)). This places the Fornax cluster at a distance of  $19.7 \text{ Mpc}$  ( $v_{\text{sys}} = 1379 \text{ km s}^{-1}$ ) and the Virgo cluster at  $15.4 \text{ Mpc}$  ( $v_{\text{sys}} = 1079 \text{ km s}^{-1}$ ), both in good agreement with SBF distances: Jerjen (2003) and Jerjen *et al.* (2004) find a Fornax distance of  $20.3 \pm 0.7 \text{ Mpc}$  and a distance of  $15.8 \pm 1.4 \text{ Mpc}$  for the Virgo M87-subcluster,

with the main uncertainty being the depth of the Virgo cluster. Using this  $H_0$  value, the NGC5044 group distance is estimated at  $35.1 \text{ Mpc}$  ( $v_{\text{sys}} = 2459 \text{ km s}^{-1}$ ), that of NGC3258 at  $40.7 \text{ Mpc}$  ( $v_{\text{sys}} = 2848 \text{ km s}^{-1}$ ), and NGC5898 at  $30.3 \text{ Mpc}$  ( $v_{\text{sys}} = 2122 \text{ km s}^{-1}$ ). Using SBF, these groups or their dominant elliptical galaxy are placed at  $31.2 \pm 4.0 \text{ Mpc}$  (NGC5044),  $32.1 \pm 4.0 \text{ Mpc}$  (NGC3258), and  $29.1 \pm 3.5 \text{ Mpc}$  (NGC5898) (Tonry *et al.* (2001)). Hence, with the exception of the NGC3258 group, Hubble-distances and SBF-distances agree within the errorbars.

Below, we discuss the position of the dEs in the (mutually dependent)  $\sigma - L_B$ ,  $R_e - L_B$ ,  $I_e - L_B$ , and  $I_e - R_e$  diagrams. Since the quantities plotted on the ordinate and abscissa are not necessarily independent (e.g.  $I_e$  and  $R_e$ ), their errors can also be correlated. We estimated the systematic and statistical (measurement) uncertainties on all quantities for a typical galaxy in our sample by assuming the values  $\sigma = 50 \pm 3 \text{ km s}^{-1}$  (assumed to be a  $1\sigma$  Gaussian error),  $R_e = 1.25 \pm 0.06 \text{ kpc}$ ,  $L_B = (8 \pm 0.8) \times 10^8 L_{\odot,B}$ . Using a Gaussian random-number generator, a data-point can be generated that is afflicted only by measurement errors. For each such new data-point, a distance estimate was generated, assuming a distance of  $30 \pm 3 \text{ Mpc}$  ( $1\sigma$ -error), which, even in the absence of other measurement errors, would introduce a correlated uncertainty on distance-dependent quantities. Each new data-point was then shifted according to its distance. We calculated 10000 new data-points for this typical galaxy, each one affected randomly by measurement errors and a distance-dependent shift. This way, the Monte-Carlo procedure properly adds the random measurement errors and the systematic distance-dependent errors. In the corner of each panel of Fig. 1, a dark grey data point is indicated, surrounded by 3000 of these simulated data points (small black dots). These give an idea of the typical systematic and statistical (correlated) errors on our data. They over-estimate the true scatter between the individual data points since all galaxies belonging to the same group or cluster will be affected in the same way by the distance uncertainty.

##### 4.1. The $\sigma - L_B$ or Faber-Jackson relation (FJR)

Bright and intermediate-luminosity ellipticals and bulges of spiral galaxies adhere closely to the FJR:  $L_B \propto \sigma^\alpha$ , with  $\alpha \sim 4$  (Faber & Jackson (1976)). Held *et al.* (1992) fitted a straight line through data of 4 dEs (three Local Group dEs and one Virgo dE) and 4 Local Group dSphs and found  $L_B \propto \sigma^{2.5}$ . They however omitted one dE from their original dataset of five and two dSphs from an original sample of six. All three deviate significantly from the relation fitted to the eight galaxies that were used, casting serious doubts on the slope of the fitted relations. PC93 fitted a straight line to the then available dE and dSph data and found  $L_V \propto \sigma^{5.6 \pm 0.9}$ . Guzmán *et al.* (1993) connected the B92 dE data with that of the dSphs and found a similar slope to the FJR of the bright ellipticals but with a different zero-point. In both attempts to measure the dE FJR, the region of about 5 magnitudes in luminosity between the dEs and the dSphs, for which no data was available, had to be bridged.

We are now for the first time in the situation that kinematical data of enough dEs are available to measure the dE FJR without the need of extrapolating towards the dSphs. Many dEs contain a central brightness peak, called the nucleus. Hence, the central velocity dispersion does not necessarily reflect the dynamics of the whole galaxy and cannot be expected to be a good measure for a galaxy's kinetic energy budget. To account for this, we instead use the luminosity-weighted mean velocity dispersion

$$\sigma = \frac{\int_0^{a_{\max}} \sigma_{\text{maj}}(a) I(a) a da}{\int_0^{a_{\max}} I(a) a da}, \quad (2)$$

with  $\sigma_{\text{maj}}(a)$  and  $I(a)$  the major-axis velocity dispersion and the surface brightness, respectively, at a major-axis distance  $a$  and  $a_{\max}$  the major-axis distance of the last kinematical data-point. Since the velocity dispersion can be strongly influenced by the nucleus and hence show a pronounced central depression, the luminosity-weighted mean velocity dispersion can differ from the central dispersion by as much as 100% of the central value. However, for  $a_{\max}$  larger than  $1 R_e$ ,  $\sigma$  changes very little by integrating farther out so we are sure that we have defined a robust quantity. For the other galaxies, we had to settle for the mean (G03) and the median (vZ04) of the dispersion profile, measured along the major axis.

As is obvious from the panel **a** in Fig. 1, the FJR becomes noticeably flatter below  $\log(L_B) \sim 9.5$  or  $M_B \sim -18.3$  mag (here and in the following,  $L_B$  is expressed using the solar B-band luminosity as unit and  $\sigma$  is expressed in units of  $\text{km s}^{-1}$ ). We fitted a straight line to the available data, taking into account the errors on the luminosities and the velocity dispersions. For the luminosities, we used  $\delta_{\log L_B} = 0.1$ . The velocity-dispersion errors  $\delta_{\log \sigma}$  of our data can be found in Table 1. For the other data sets, we of course used the errors stated by the various authors. We minimized the non-linear quantity

$$\chi^2 = \frac{1}{N-2} \sum_{i=1}^N \frac{(a + b \log \sigma_i - \log L_{Bi})^2}{b^2 \delta_{\log \sigma_i}^2 + \delta_{\log L_{Bi}}^2}, \quad (3)$$

with  $\log \sigma_i$  and  $\log L_{Bi}$  observed data-points and  $\delta_{\log \sigma_i}$  and  $\delta_{\log L_{Bi}}$  the corresponding errorbars, using the routine `fitexy` of Press *et al.* (1992) in order to obtain the zeropoint  $a$  and the slope  $b$ .  $N$  is the number of data points. The diagonal elements of the estimated covariance matrix were used as approximations to the variances of the regression coefficients  $a$  and  $b$ . A straight-line fit to the DR04, vZ04, G03, and B92 dEs yields

$$\log L_B = 6.02^{\pm 0.31} + 1.57^{\pm 0.19} \log \sigma \quad (4)$$

with a regression coefficient  $r = 0.68$  and  $\chi^2 = 4.9$ . If the B92 dSphs are included in the fit, one obtains

$$\log L_B = 4.39^{\pm 0.37} + 2.55^{\pm 0.22} \log \sigma \quad (5)$$

with a regression coefficient  $r = 0.85$  and  $\chi^2 = 9.2$ . The linear trend becomes more significant since a much larger data-interval is covered but the  $\chi^2$  is much higher, quantifying what the eye sees immediately: the  $\sigma - L_B$  relation does not have a constant slope when going from the dEs to the dSphs. A dE

FJR that is steeper than the FJR of bright ellipticals is definitely excluded by these data. This clearly shows the need of combining the available data-sets of dE kinematics and the dangers involved with extrapolating each of these data-sets separately towards the dSphs. Moreover, these results contradict the universality of the  $\sigma - L_B$  relation, which was suggested by Guzmán *et al.* (1993). A currently running project on the properties of faint early-type galaxies ( $-22 < M_R < -17.5$ ) in the central 1deg of the Coma cluster yields FJR  $L \propto \sigma^{2.01}$  at the faint end, which is consistent with our results (Matković & Guzmán, private communication).

According to the YA87 models, if a mass-fraction  $f$  is blown away, a galaxy evolves to a new virial equilibrium with a velocity dispersion that is offset from the initial value by

$$\Delta \log \sigma = \log(1 - f) \quad (6)$$

for slow, and

$$\Delta \log \sigma = 0.5 \log(1 - 2f), \quad (7)$$

for instantaneous mass-loss.

Hence, the expansion following the galactic wind drives more low-mass dEs, that lose a larger mass-fraction than more massive objects, progressively towards lower velocity dispersions, leading to a flatter FJR in the luminosity regime of the dEs (cf. the shift with respect to the zero mass-loss curve of the evolutionary endpoints of a typical  $m_B = 16$  Fornax dE, indicated by white circles in Fig. 1). Galaxies with luminosities in the range  $\log L_B \approx 4.4 - 8.2$  ( $M_B = -5.5$  to  $-15.0$  mag) are disrupted by the instantaneous ejection of more than half of their initial mass which causes the velocity dispersion to drop to zero at  $\log L_B \approx 8.2$  ( $M_B = -15.0$  mag). The locus of the dEs in a  $\log L_B$  versus  $\log \sigma$  diagram is bracketed nicely by the lines corresponding to slow and instantaneous mass-loss. The zero mass-loss YA87  $\sigma - L_B$  relation has a slope similar to that of the bright ellipticals although it underestimates the velocity dispersion of the very brightest ellipticals (most likely due to the fact that mergers are not taken into account). The CC02 models A collapse to rather centrally concentrated systems with velocity dispersions that are about a factor two too high. The CC02 models B agree with the YA87 models for slow mass-loss and also reproduce the observations fairly well, from the dSphs up to the brightest ellipticals. For a comparison of the FJR with SAM-predictions, with and without dynamical response to mass loss, see Figs. 12 and 14, respectively, of NY04.

#### 4.2. The $R_e - L_B$ relation or Fish's law

According to the YA87 models, galaxies experiencing mass-loss are expected to evolve towards larger half-light radii at fixed luminosity, i.e. to the right in panel **b** of Fig. 1, which relates the half-light radius (in kpc) to luminosity, by an amount

$$\Delta \log R_e = -\log(1 - f) \quad (8)$$

for slow, and

$$\Delta \log R_e = \log(1 - f) - \log(1 - 2f), \quad (9)$$

for instantaneous loss of a mass-fraction  $f$ . Galaxies in the luminosity range  $\log L_B \approx 4.4 - 8.2$  ( $M_B \approx -5.5$  to  $-15.5$  mag)

are disrupted by the instantaneous loss of more than half of their initial mass. This causes their half-light radius to diverge at  $\log L_B \approx 8.2$  ( $M_B \approx -15$  mag). The zero mass-loss  $L_B - R_e$  relation predicted by YA87 (i.e. the sequence that galaxies would trace if the dynamical response to the mass loss is not taken into account) is slightly steeper than that of the bright elliptical galaxies and the very brightest elliptical galaxies have larger half-light radii than is expected. The slope of the zero mass-loss relation in combination with the dynamical response to the galactic wind result in a dE  $L_B - R_e$  relation that is much steeper than that of the brighter galaxy species, as is actually observed. For bulges, intermediate-luminosity and bright ellipticals, the best fitting straight line is given by  $L_B \propto R_e^{1.19}$  (Guzmán *et al.* (1993)).

For the dEs, we used the same non-linear least-squares technique as in the previous section, assuming an error of 5% on the DR04 effective radii. This error takes into account the error on the measurement of the total magnitude and photon-shot noise. It should be noted that not all authors measure effective radii the same way. In DR04,  $R_e$  is the radius  $R_{e,\text{circ}}$  of the circular aperture that encloses half the light. Ba03 and Gr03 use the geometric mean radius  $R_{e,\text{mean}}$  (which is not expected to deviate much from  $R_{e,\text{circ}}$ ). G03 uses the major-axis distance  $R_{e,\text{maj}}$  as radius. We derived geometric mean half-light radii from the G03 data using the relation  $R_{e,\text{mean}} = \sqrt{1 - \epsilon} R_{e,\text{maj}}$ , with  $\epsilon$  the ellipticity. The B92 are a mix of  $R_{e,\text{circ}}$  and  $R_{e,\text{mean}}$  measurements. A fit to the DR04, G03, and B92 dEs yields

$$\log L_B = 8.72^{\pm 0.04} + 2.07^{\pm 0.26} \log R_e \quad (10)$$

with a regression coefficient  $r = 0.68$  and  $\chi^2 = 5.1$ . Taking the dSphs together with these dEs makes the slope even steeper:

$$\log L_B = 8.50^{\pm 0.05} + 3.71^{\pm 0.20} \log R_e \quad (11)$$

with a regression coefficient  $r = 0.90$  and  $\chi^2 = 8.2$ . One should be very cautious about these results since adding the Ba03 dEs clearly destroys the impression of a strong linear relation. Also, the YA87 models do not predict that a tight  $L_B - R_e$  relation should exist, given the spread between the models with slow and instantaneous mass-ejection (unlike in the case of the  $\sigma - L_B$  relation where slow and instantaneous mass-loss models almost coincide in the dE-regime). The slope of the dE/dSph  $L_B - R_e$  relation is reproduced very nicely by the CC02 models, although the models of series A, that virialized at high redshift, are too compact while the models of series B, that virialized at low redshift, are too extended. This however does not necessarily invalidate these calculations nor the wind model since the initial density of the models, and hence the present-day half-light radius to which they collapse, depends on the virialization redshift which was arbitrarily fixed at  $z = 5$  by Chiosi & Carraro (2002). These authors argue that, interpolating between the CC02 models A and B, models that virialized at  $z \sim 2$  would be able to reproduce the position of dEs in this diagram.

The locus of the observed dEs is bracketed by the YA87 models for slow and instantaneous gas removal. The K01 models roughly agree with the observations and with the YA87 models. SAMs (like NY04) predict some cosmic scatter on

structural scaling relations because of the different merger trees that lead up to a galaxy with a given present-day luminosity. K01 only calculated one model per mass per feedback efficiency. It is therefore not possible to assess the uncertainty on (or the scatter about) the predicted model properties. Still, it is encouraging that the models with minimal feedback efficiency approximate the zero or slow mass-loss models of YA87 while the models with high feedback efficiency expand towards larger half-light radii, reproducing the onset of the dE sequence. For a comparison of the  $L_B - R_e$  relation with SAM-predictions see Fig. 10 of NY04.

#### 4.3. The $I_e - L_B$ relation

The YA87 models predict that galaxies should expand after the galactic-wind phase and evolve towards a more diffuse state, characterised by a much lower surface brightness. Hence, they should move to the left in panel **c** of Fig. 1, which relates surface brightness to total luminosity, by an amount

$$\Delta \log I_e = 2 \log(1 - f) \quad (12)$$

for slow, and

$$\Delta \log I_e = 2 \log(1 - 2f) - 2 \log(1 - f), \quad (13)$$

for instantaneous mass-loss. Galaxies in the luminosity range  $\log L_B \approx 4.4 - 8.2$  ( $M_B \approx -5.5$  to  $-15.5$  mag) become unbound after the instantaneous loss of more than half of their initial mass and consequently evolve towards zero surface brightness. In the range  $\log L_B = 7 - 11$  ( $M_B = -12$  to  $-22$  mag), the zero mass-loss  $I_e - L_B$  relation runs almost vertically in this diagram, predicting that  $\log I_e \approx 2.5$  for all elliptical galaxies. While most intermediate-luminosity ellipticals indeed scatter around this value, bright elliptical galaxies tend to be more diffuse, with surface brightnesses in the range  $\log I_e \approx 2.0 - 2.5$ . Since less massive galaxies are expected to lose a larger mass-fraction than more massive objects, they move progressively towards lower surface brightnesses, changing the slope of the  $I_e - L_B$  relation. The YA87 models for slow and instantaneous mass-loss are able to reproduce the observed trend in the  $I_e - L_B$  diagram, with the dE-sequence running almost perpendicular to that of the bright galaxies. The faintest K01 models also coincide with the observed locus of the dEs. The CC02, being either too diffuse or too compact depending on the virialization redshift, end up having too high or too low surface brightness (see the discussion in subsection 4.2). However, they roughly reproduce the slope of the observed dE sequence. For a comparison of the  $L_B - I_e$  relation with SAM-predictions see Fig. 9 of NY04.

#### 4.4. The $R_e - I_e$ or Kormendy relation

The 12 dEs in the B92 sample suggest a  $R_e - I_e$  relation that runs almost perpendicular to that of the bright ellipticals and bulges (Guzmán *et al.* (1993)). However, this picture changes completely when more data, especially of faint galaxies, are added, as is obvious from panel **d** in Fig. 1. This result was already derived by e.g. Capaccioli *et al.* (1992) and Graham *et al.* (2003).

Mass-loss moves galaxies towards larger half-light radii and towards much lower surface brightnesses, i.e. slightly to the right and steeply downward with respect to the initial  $\log R_e$ - $\log I_e$  relation, by an amount given by equations (8) and (12) for slow, and equations (9) and (13) for instantaneous loss of a mass-fraction  $f$ . The region occupied by models that are disrupted by instantaneous gas ejection is bounded by the leftmost and rightmost thick grey lines in panel **d** of Fig. 1. The position of a typical  $m_B = 16$  Fornax dE before and after slow or fast gas removal is indicated by white circles in Fig. 1, showing the direction in which dEs are expected to evolve in this diagram. The slope of the dE  $R_e$ - $I_e$  relation (if it can be called such, given the large scatter) is nicely reproduced by these models. The  $R_e$ - $I_e$  relation predicted by YA87 becomes much flatter in the regime of the intermediate-luminosity and bright elliptical galaxies. However, the very brightest elliptical galaxies have larger half-light radii and hence lower surface brightnesses than accounted for by the YA87 relation, due to not taking into account the fact that mergers played an important role in shaping bright ellipticals. Again, the CC02 models are either too compact or too extended. They roughly reproduce the trend going from dEs towards dSphs. The photometric properties of the K01 models agree rather well with the observations. The effect of the kinetic feedback efficiency of supernova explosions is clear: models with a low feedback efficiency (top sequence of K01 models in panel **d** of Fig. 1) experience a late galactic wind and lose little gas. Consequently, the dynamic response is rather mild and they scatter about the YA87 zero mass-loss curve. Models with a high feedback efficiency (bottom sequence in panel **d** of Fig. 1) lose much more gas and expand towards much larger  $R_e$  and lower  $I_e$ . At fixed mass but for different feedback efficiencies, the trend is in the same direction as the observed  $R_e$ - $I_e$  relation and as the YA87 models (with feedback efficiency replaced with mass-loss timescale). For a comparison of the Kormendy relation with SAM-predictions see Fig. 11 of NY04.

## 5. Bivariate relations

### 5.1. The Fundamental Plane (FP)

The FP of the bulges and the bright and intermediate-luminosity ellipticals is given by the equation

$$\log R_e = \text{const.} + 1.14 \log \sigma - 0.785 \log I_e, \quad (14)$$

(Guzmán *et al.* (1993)). The FP can be seen as an emanation of the virial theorem, relating the potential energy  $\mathcal{PE}$  and kinetic energy  $\mathcal{KE}$  budgets of a galaxy in equilibrium. More specifically, with  $\mathcal{PE} = GM^2/R_G$  and  $\mathcal{KE} = \frac{1}{2}M\langle v^2 \rangle$ , where  $M$  is the mass of the galaxy,  $R_G$  its gravitational radius, and  $\langle v^2 \rangle$  the mass-weighted mean-square stellar velocity (see Binney & Tremaine (1987)), one finds that  $\mathcal{PE} + 2\mathcal{KE} = 0$  or that  $M \propto R_G\langle v^2 \rangle$ . Hence, one expects that  $M = c R_e \sigma^2$ , with  $c$  a proportionality parameter that (hopefully) transforms the mass-weighted theoretical parameters ( $R_G$ ,  $\sqrt{\langle v^2 \rangle}$ ) to the luminosity-weighted observed ones ( $R_e$ ,  $\sigma$ ). This, together with the relation  $L_B = 2\pi I_e R_e^2$ , leads to the theoretical FP relation

$$\log R_e = \text{const.} + \log c - \log \frac{M}{L} + 2 \log \sigma - \log I_e. \quad (15)$$

Variations of  $c$  (structural non-homology) and/or the mass-to-light ratio  $M/L$  along the mass sequence of dynamically hot galaxies, exacerbated by an imperfect correspondence between  $\sigma$  and  $\sqrt{\langle v^2 \rangle}$  due to rotation and anisotropy, slightly change the tilt of the FP to the observed value and introduce some scatter (see e.g. Trujillo *et al.* (2004)).

The positions of the various galaxy species in a side view of the FP are plotted in Fig. 2. We did not correct our velocity dispersions for aperture effects in this plot since applying the prescriptions given by Blakeslee *et al.* (2002) leads to corrections of order  $\Delta \log \sigma = 0.02$  and are clearly negligibly small. In both panels of Fig. 2, a cloud of 3000 simulated data points, calculated along the lines discussed in section 4, is plotted to give an idea of the systematic and statistical uncertainty on a typical DR04 data point (indicated by a grey dot). Here and in the following, we have also made use of the FP-data of 14 Coma cluster dEs presented by Guzmán *et al.* (2003) (Gu03). By and large, dEs show a tendency to lie above the FP in this projection. The Local Group dSphs deviate even more extremely from the FP. The dynamical response after the loss of a mass-fraction  $f$ , given by

$$\begin{aligned} \Delta(-0.785 \log I_e + 1.14 \log \sigma) &= -0.43 \log(1-f), \\ \Delta \log R_e &= -\log(1-f), \end{aligned} \quad (16)$$

for slow removal and

$$\begin{aligned} \Delta(-0.785 \log I_e + 1.14 \log \sigma) &= 1.57 \log(1-f) \\ &\quad - \log(1-2f), \\ \Delta \log R_e &= \log(1-f) - \log(1-2f), \end{aligned} \quad (17)$$

for instantaneous mass-loss, moves dEs almost parallel to the FP in the direction of larger half-light radii (see e.g. the typical  $m_B = 16$  Fornax dE which moves from left to right, as shown by the white circles in Fig. 2). Since the zero mass-loss FP has a much flatter slope than the observed one, fainter galaxies are indeed expected to lie progressively above the FP in this projection. The CC02 models A agree very well with the YA87 models and with the observations. The surface brightness of the CC02 models B however is much lower than observed, placing them well above the observed FP in this projection.

In the right panel of Fig. 2, the deviations of the different galaxy species from the FP are plotted as a function of luminosity. The expected change of the FP residual after the ejection of a mass fraction  $f$  is given by

$$\Delta((-0.785 \log I_e + 1.14 \log \sigma) - \log R_e) = 0.57 \log(1-f), \quad (18)$$

i.e. slightly downwards with respect to the YA87 zero mass-loss sequence, which itself is a steep function of luminosity. This expression is valid both for slow and instantaneous winds although in the latter case galaxies in the luminosity range  $\log L_B \approx 4.4 - 8.2$  ( $M_B \approx -5.5$  to  $-15.5$  mag) cease to exist. Hence, according to the YA87 calculations, the dynamical response after mass-loss in fact reduces the FP residual. Still, dEs are expected to lie above the FP in this projection. The YA87 and the CC02 models A roughly reproduce the observed trend

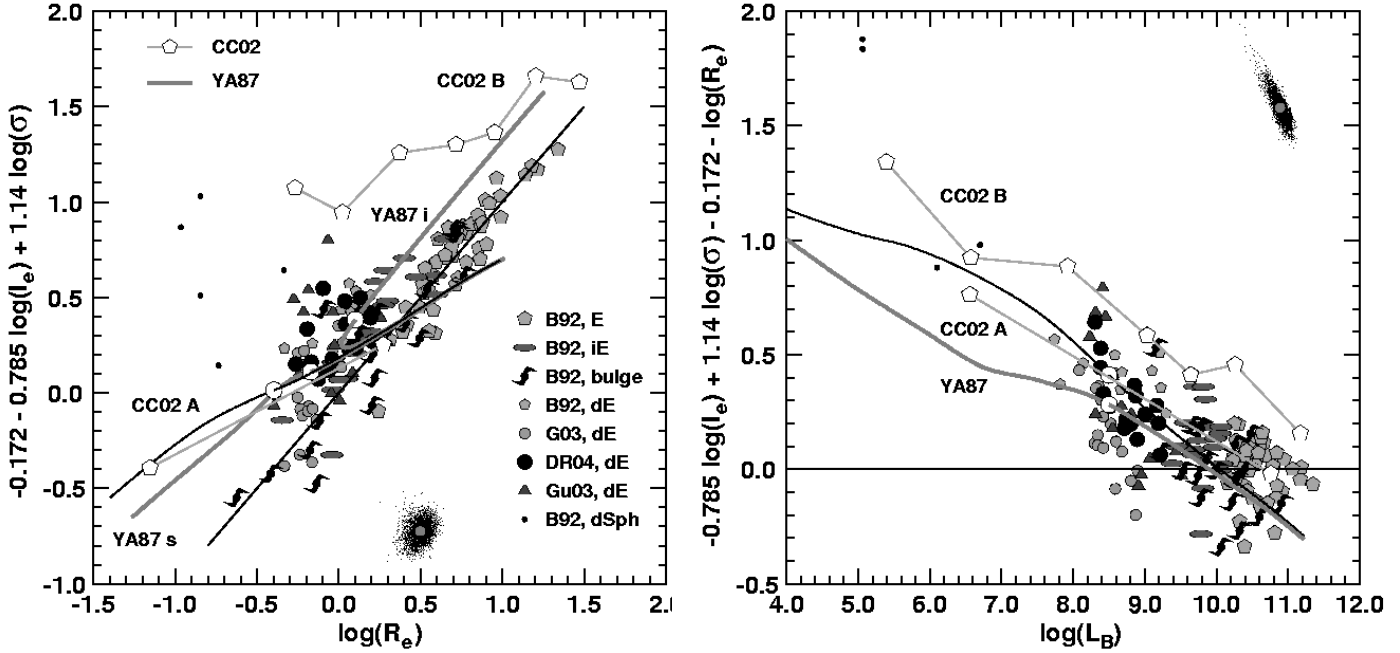


**Fig. 2.** Left panel: an edge-on view onto the FP of the bulges, bright and intermediate-luminosity ellipticals in  $(\log R_e, \log I_e, \log \sigma)$  space. All symbols have the same meaning as in Fig. 1. The straight black line traces the  $\log R_e = -0.172 - 0.785 \log I_e + 1.14 \log \sigma$  relation that defines the FP. The dEs observed by Guzmán *et al.* (2003) (Gu03) have been added to the DR04, G03, and B92 data sets. The curved black line traces the FP of the zero mass-loss YA87 models. The thick grey lines give the locus of the YA87 models after slow (bottom thick grey line) or fast (top thick grey line) gas removal. The white circles show the expected evolution of a  $m_B = 16$  Fornax dE: most of the evolution happens almost parallel to the FP so that, given the slope of the zero mass-loss YA87 FP, one would expect dEs to lie slightly above the FP defined by the bright ellipticals in this projection. Right panel: vertical deviation of the FP as a function of luminosity. All models predict less massive galaxies to lie progressively higher above the FP in this projection, as is observed. The YA87 curves for slow and instantaneous winds coincide in this diagram. In each panel, a cloud of 3000 simulated data points is plotted to give an idea of the systematic and statistical uncertainty on a typical DR04 data point (indicated by a grey dot).

as a function of  $\log L_B$ . The CC02 models of series B show approximately the same trend but lie systematically above the FP in this projection.

## 5.2. The FP in $\kappa$ -space

Another way to view the FP is in the so-called  $\kappa$ -space (Bender *et al.* (1992)) defined by

$$\begin{aligned} \kappa_1 &= \frac{1}{\sqrt{2}} \log(R_e \sigma^2), \quad \kappa_2 = \frac{1}{\sqrt{6}} \log\left(\frac{I_e^2 \sigma^2}{R_e}\right), \\ \kappa_3 &= \frac{1}{\sqrt{3}} \log\left(\frac{\sigma^2}{I_e R_e}\right). \end{aligned} \quad (19)$$

Using these definitions and the virial theorem,  $\kappa_1$  is expected to be a measure for the mass of a galaxy,  $\kappa_2$  is sensitive mostly to surface brightness and  $\kappa_3$  depends on the mass-to-light ratio. A galaxy is shifted in  $\kappa$ -space by an amount

$$\begin{aligned} \Delta\kappa_1 &= \frac{1}{\sqrt{2}} \log(1-f), \quad \Delta\kappa_2 = \frac{7}{\sqrt{6}} \log(1-f), \\ \Delta\kappa_3 &= \frac{1}{\sqrt{3}} \log(1-f) \end{aligned} \quad (20)$$

if a mass-fraction  $f$  is blown away in a slow wind. An instantaneous wind engenders a dynamical response given by

$$\begin{aligned} \Delta\kappa_1 &= \frac{1}{\sqrt{2}} \log(1-f), \\ \Delta\kappa_2 &= \frac{1}{\sqrt{6}} (6 \log(1-2f) - 5 \log(1-f)), \\ \Delta\kappa_3 &= \frac{1}{\sqrt{3}} \log(1-f). \end{aligned} \quad (21)$$

Since a galaxy's luminosity is not affected by the ejection of gas,  $I_e \propto R_e^{-2}$ , and

$$\Delta\kappa_1 \propto \Delta\kappa_3 \propto \Delta \log M. \quad (22)$$

Galaxies are therefore expected to evolve downwards and to the left in the  $(\kappa_1, \kappa_3)$ -projection of the FP (left panel of Fig. 3). In both panels of Fig. 3, a cloud of 3000 simulated data points, calculated along the lines discussed in section 4, is plotted to give an idea of the systematic and statistical uncertainty on a typical DR04 data point (indicated by a grey dot). The YA87 zero mass-loss FP however has a much flatter slope than the observed FP, which tends to position dEs slightly above the FP in this projection. As in the right panel of Fig. 2, the dynamical

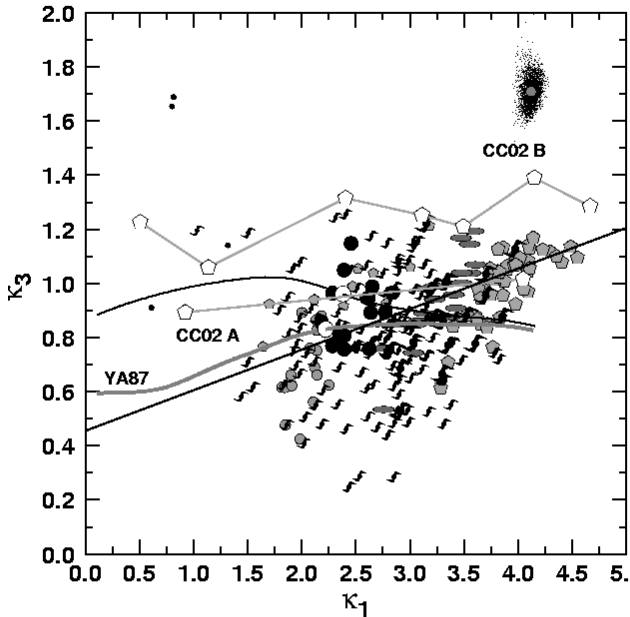
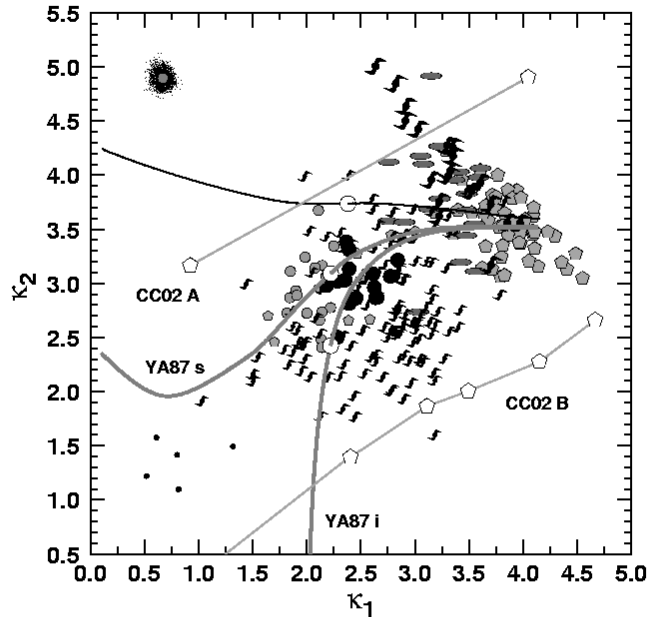


**Fig. 3.** The FP in  $\kappa$ -space. Left panel: edge-on view of the FP, the black straight line traces the  $\kappa_3 = 0.46 + 0.15\kappa_1$  relation. All symbols have the same meaning as in Fig. 1. The Sc/Sd/Irr galaxies taken from Burstein *et al.* (1997) are plotted as small spirals. According to the YA87 models, the evolution in the  $(\kappa_1, \kappa_3)$  plane does not depend on the time-scale on which mass is lost as a galactic wind. The predicted tendency for faint dwarf galaxies to lie above the FP in this projection is borne out by the observations. Right panel: face-on view onto the FP (equivalent to panel c of Fig. 1). The evolution within the FP is much more outspoken: the mass-loss suffered by the dwarf galaxies makes them expand, shifting them towards lower  $\kappa_2$  values. The dEs and dSphs end up forming a sequence almost parallel to that of the bulges and the bright and intermediate-luminosity ellipticals. The CC02 models A reproduce the slope of the dE FP but are somewhat too compact and as a consequence have too high  $\kappa_2$  values. The CC02 models B on the contrary are too extended lie below the dE sequence in the  $(\kappa_1, \kappa_2)$  plane. In each panel, a cloud of 3000 simulated data points is plotted to give an idea of the systematic and statistical uncertainty on a typical DR04 data point (indicated by a grey dot).

response to the galactic wind moves galaxies away from the zero mass-loss FP towards the FP of the bright galaxies.

The sensitivity of  $\kappa_2$  to surface brightness, which drops significantly as a galaxy expands after the wind phase, leads to a strong downward evolution in the  $(\kappa_1, \kappa_2)$ -projection of the FP (right panel of Fig. 3). The models undergoing an instantaneous wind are disheveled most severely by the suffered mass-loss and show the most pronounced evolution in the  $(\kappa_1, \kappa_2)$  plane. The YA87 models and the CC02 models A are able to reproduce the position of the dEs in the  $(\kappa_1, \kappa_3)$ -projection of the FP. The CC02 models B are too extended and consequently lie above the observed FP in this projection. In the  $(\kappa_1, \kappa_2)$ -projection, which is a nearly face-on view onto the FP, the dEs define a sequence running almost perpendicular to that of the bulges and the bright and intermediate-luminosity ellipticals. Within the context of the YA87 models, this is in part due to the zero mass-loss sequence which runs almost horizontally across the  $(\kappa_1, \kappa_2)$ -plane and to the evolution induced by the mass-loss during the galactic-wind phase, which shifts galaxies downwards. Both the YA87 and the CC02 models reproduce the observed slope of the dE sequence in the  $(\kappa_1, \kappa_2)$ -plane.

The present-day Sc/Sd/Irr galaxies are probably the stellar systems that best resemble the dE progenitors as envisaged



by the harassment scenario. Their position in  $\kappa$ -space, with the maximum rotation velocity  $v_{\max}$  used as a substitute for the theoretical quantity  $\sqrt{\langle v^2 \rangle}$  in the virial theorem, is indicated in Fig. 3 by small spiral symbols. This population of late-type galaxies has a much larger scatter in  $\kappa$ -space than the dEs. It is not clear how harassment, which is by nature a stochastic process whose effects depend in a very complicated way on the orbit of a progenitor galaxy through a given galaxy cluster or group, could transform the scatter cloud of late-types into the much tighter dE sequence.

## 6. Discussion and conclusions

We have presented the sequences traced by dEs in the  $\log L_B$  vs.  $\log \sigma$ ,  $\log L_B$  vs.  $\log R_e$ ,  $\log L_B$  vs.  $\log I_e$ , and  $\log R_e$  vs.  $\log I_e$  diagrams and in the  $(\log \sigma, \log R_e, \log I_e)$  parameter space in which bright and intermediate-luminosity elliptical galaxies and bulges of spirals define a Fundamental Plane (FP). These results are based on three equally large kinematical data-sets: the data presented in this paper (DR04), G03, and vZ04. This brings the number of dEs with resolved kinematics to 43. More data were added when studying correlations involving only photometric data (Ba03 and Gr03) or the FP (Gu03). We

also used the kinematical and photometric data presented in B92. Our main conclusions are the following:

- We have shown that the  $\sigma - L_B$  or Faber-Jackson relation does *not* have a constant slope when going from the bright ellipticals, over the dEs, down to the dSphs, contrary to previous claims. The  $L_B \propto \sigma^{3.7}$  relation of the bright galaxies changes into a  $L_B \propto \sigma^{1.6 \pm 0.2}$  relation below  $L_B \approx 9.4$  ( $M_B \approx -18$  mag). A dE FJR as steep as or even steeper than that of the bright ellipticals is definitely excluded by these data. A flatter slope is predicted by all models presented here (YA87, CC02) as a consequence of the dynamical response to the supernova-driven gas ejection. More sophisticated SAMs that simulate the hierarchical merger tree that leads up to the formation of a galaxy show that post-merger starbursts are absolutely necessary to bring the models in agreement with a whole host of observations and that a significant flattening of the FJR in the dE-regime is a direct consequence of the dynamical response to starburst-induced gas ejections (Somerville *et al.* (2001), Nagashima & Yoshii (2004)). As a consequence, dEs and their progenitors, being low-mass, fragile objects, are the ideal objects to study if one aims at further refining prescriptions for star-formation, supernova feedback and the response to galactic winds in semi-analytical or numerical simulations of cosmological structure growth. It should be noted however that gas-rich dwarf late-type galaxies exist whose large H $\alpha$  content appears to be at variance with CDM predictions (Mayer & Moore (2004)). It is not clear yet how worrisome this actually is and, since we restrict ourselves to the properties of gas-poor dEs, a discussion of the H $\alpha$  properties of dwarf late-type galaxies is clearly beyond the scope of this paper.
- The simple fact that these diffuse, low surface-brightness, low velocity-dispersion dEs exist puts strong constraints on the redshift dependence of the cosmic star-formation rate. Nagashima & Yoshii (2004) have shown convincingly that structure-formation models in a  $\Lambda$ CDM universe with a short star-formation timescale at high  $z$  fail to produce such inflated dEs. In such a universe, dEs are assembled from progenitors that have already converted most of their gas into stars, and they are expected to trace the same sequences in the panels of Fig. 1 as the giant ellipticals (which are formed further down the merger tree from almost purely stellar progenitors, independent of the cosmic star-formation rate). Only models that have long enough star-formation timescales at high  $z$ , such that dEs can be formed by the mergers of gaseous progenitors, agree with these observations (e.g. the models of NY04 with a redshift independent star-formation time scale  $\tau_* = 1.3$  Gyr, where the star-formation rate is given by  $M_{\text{gas}}/\tau_*$  with  $M_{\text{gas}}$  the H $\alpha$  mass). The starburst triggered by each merger and the ensuing supernova-explosions eject gas and thus lead to a population of diffuse dwarf galaxies with low velocity dispersions, as observed. This also explains the success of the YA87 and CC02 models, which do not take into account mergers but rather assume galaxies to originate from a single gas cloud, for dEs while they fail to reproduce the properties of massive ellipticals.
- However, all this needs to be reconciled with the observation that the stellar mass density of the universe at redshift  $z > 2$ , contained in massive galaxies, is larger than can be accounted for by SAMs (Fontana *et al.* (2003), Somerville *et al.* (2004)). Still, the distribution of the dEs in the various univariate diagrams can, if enough dwarf galaxies have been observed for statistically sound statements to be made, put very stringent limits on the redshift dependence of the star-formation timescale in semi-analytical or numerical simulations of galaxy evolution.
- Models for the evolution of dwarf and intermediate-luminosity elliptical galaxies, based on the idea that these stellar systems grow from collapsing primordial density fluctuations, are able to reproduce the observed relations between parameters that quantify their structure ( $L_B$ ,  $R_e$ ,  $I_e$ ) and internal dynamics ( $\sigma$ ) quite well. Despite their simplicity, the YA87 models account very well for the behaviour of dEs in the  $(\log \sigma, \log R_e, \log I_e)$  parameter space. Although numerically and physically much more sophisticated and with a more sound cosmological footing, the predictions of the models presented by K01 and Nagashima & Yoshii (2004) agree with the YA87 models. The CC02 models, in which the virialization redshift of the models is set “by hand”, fail to get the zeropoints correctly but nonetheless are able to reproduce the slopes of the various relations. All this suggests that little merging took place in the life of a dE *after* it started forming stars.
- Low-mass systems such as dEs and dSphs lie above the FP in the projection used in Figs. 2 and 3 defined by the bright ellipticals, with fainter galaxies lying progressively higher above the FP. It is well known that the remnant of the merger of two galaxies is more diffuse than its progenitors (see e.g. Hernquist (1992) and Dantas *et al.* (2003) for dissipationless mergers and Hernquist *et al.* (1993) and Bekki (1998) for merger simulations taking into account the presence of gas). Hence, the structural properties of the brightest elliptical galaxies, including the slope of the FP, can be explained quite well if late mergers (with progenitors that had already converted a significant fraction of their gas into stars) played an important role in their formation and evolution. This is much less the case for less massive systems such as dEs, which formed higher up the hierarchical merging tree from more dissipative mergers.
- While dEs follow well-defined sequences in the various univariate diagrams, the correlations are not as tight as in the case of bright ellipticals. This cannot only be due to measurement uncertainties (e.g. very deep photometry is now available that allows to determine  $L_B$  and  $R_e$  with very small errors, still the scatter on the dE  $\log R_e$ - $\log I_e$  relation is large). This cosmic scatter may be a consequence of the sensitivity of these low-mass systems to both internal (supernova explosions, feedback efficiency, the details of galactic winds, ...) and external processes (gravitational interactions, tidal stripping of stars and ram-pressure stripping of gas, ...) in group and cluster environments. Hence, these objects are ideal laboratories to study these physical

processes to which bright ellipticals seem to be quite insensitive.

- The wind model has passed this test. However, these findings do not necessarily falsify the harassment scenario. The dEs observed so far overlap in  $\kappa$ -space (see Fig. 3) with the present-day analogs of possible dE progenitors (the Scd and Irr galaxies). This overlap leaves open the possibility that we have observed dEs that formed via hierarchical merging *and* dEs that formed via harassment. Especially since some of the dEs observed during the Large Program provide us with very strong evidence (such as embedded stellar disks or kinematically decoupled cores) that harassment has indeed played an important role in their past evolution.

Hence, judging from the photometric and kinematical data that are now available, dEs are most likely a mixed population, with primordial and more recently (trans)formed objects co-existing in the present-day universe. More spectroscopic age and metallicity estimates and kinematical data are required in order to allow the importance of the evolutionary avenues to be constrained, especially of faint, low surface-brightness dEs in order to fill the gap between the dEs and the dSphs in the FJR (the faintest dEs with resolved kinematics are still  $\sim 20$  times brighter than the brightest Local Group dSph) and to determine the position of such faint dEs in the other uni- and bivariate diagrams.

**Acknowledgements.** Based on observations made at the European Southern Observatory, Chile (ESO Large Programme Nr. 165.N-0115). SDR wishes to thank Philippe Prugniel for fruitful discussions while visiting the CRAL-Observatoire de Lyon. WWZ acknowledges the support of the Austrian Science Fund (project P14753). DM acknowledges the support of the Bijzonder OnderzoeksFonds (BOF Universiteit Gent). This research has made use of the NASA/IPAC Extragalactic Database (NED) which is operated by the Jet Propulsion Laboratory, California Institute of Technology, under contract with the National Aeronautics and Space Administration.

## References

Barazza, F. D., Binggeli, B., & Jerjen, H., 2002, *A&A*, 391, 823  
 Barazza, F. D., Binggeli, B., Jerjen, H., 2003, *A&A*, 127, 771 (Ba03)  
 Bekki, K., 1998, *ApJ*, 496, 713  
 Bender, R., Surma, P., Döbereiner, S., Möllenhoff, C., Madejsky, R., 1989, *A&A*, 217, 35  
 Bender, R., Burstein, D., Faber, S. M., 1992, *ApJ*, 399, 462 (B92)  
 Binggeli, B., Sandage, A., Tarenghi, M., 1984, *AJ*, 89, 64  
 Binney, J. & Tremaine, S., 1987, “Galactic Dynamics”, Princeton University Press, New Jersey, US  
 Blakeslee, J. P., Lucey, J. R., Tonry, J. L., Hudson, M. J., Narayanan, V. K., Barris, B. J., 2002, *MNRAS*, 330, 443  
 Burstein, D., Bender, R., Faber, S. M., Nolthenius, R., 1997, *AJ*, 114, 1365  
 Butcher, H. & Oemler, A., 1978, *ApJ*, 219, 18  
 Capaccioli, M., Caon, N., D’Onofrio, M., 1992, *MNRAS*, 259, 323  
 Chiosi, C. & Carraro, G., 2002, *MNRAS*, 335, 335 (CC02)  
 Dantas, C. C., Capelato, H. V., Ribeiro, A. L. B., de Carvalho, R. R., 2003, *MNRAS*, 340, 398  
 De Rijcke, S., Dejonghe, H., Zeilinger, W. W., & Hau, G. K. T., 2001, *ApJ*, 559, L21  
 De Rijcke, S., Dejonghe, H., Zeilinger, W. W., & Hau, G. K. T., 2003, *A&A*, 400, 119  
 De Rijcke, S., Zeilinger, W. W., Dejonghe, H., & Hau, G. K. T., 2003, *MNRAS*, 339, 225  
 De Rijcke, S., Dejonghe, H., Zeilinger, W. W., & Hau, G. K. T., 2004, accepted by *A&A*, astro-ph/0407425  
 Djorgovski, S. & Davis, M., 1987, *ApJ*, 313, 59  
 Dressler, A., Faber, S. M., Burstein, D., Davies, R. L., Lynden-Bell, D., Terlevich, R., Wegner, G., 1987, *ApJ*, 313, L37  
 Duc, P.-A., Bournaud, F., Masset, F., *A&A*, 427, 803  
 Faber, S. M. & Jackson, R. E., 1976, *ApJ*, 204, 668  
 Falcón-Barroso, J., Peletier, R. F., Vazdekis, A., Balcells, M., 2003, *ApJ*, 588, L17  
 Ferguson, H. C., 1989, *AJ*, 98, 367  
 Ferguson, H. C., & Binggeli, B., 1994, *A&A Rev.*, 6, 67  
 Ferguson, H. C., Sandage, A., 1990, *AJ*, 101, 765  
 Fish, R. A., 1963, *AJ*, 68, 72  
 Fish, R. A., 1964, *ApJ*, 139, 284  
 Fontana, A., Donnarumma, I., Vanzella, E., Giallongo, E., Menci, N., Nonino, M., Saracco, P., Cristiani, S., D’Odorico, S., Poli, F., 2003, *ApJ*, 593, L9  
 Forbes, D. A., Ponman, T. J., Brown, R. J. N., 1998, *ApJ*, 508, L43  
 Freedman, W. L., Madore, B. F., Gibson, B. K., Ferrarese, L., Kelson, D. D., Sakai, S., Mould, J. R., Kennicutt, R. C., Jr., Ford, H. C., *et al.*, 2001, *ApJ*, 553, 47  
 Geha, M., Guhathakurta, P., van der Marel, R. P., 2003, *AJ*, 126, 1794 (G03)  
 Gerhard, O. E., 1993, *MNRAS*, 265, 213  
 Graham, A. W., Jerjen, H., Guzmán, R., 2003, *AJ*, 126, 1787  
 Graham, A. W., Guzmán, R., 2003, *AJ*, 125, 2936  
 Guzmán, R., Lucey, J. R., Bower, R. G., 1993, *MNRAS*, 265, 731  
 Guzmán, R., Graham, A. W., Matkovic, A., Vass, I., Gorgas, J., Cardiel, N., 2003, “Star Formation Through Time”, *ASP Conf. Proc.*, Vol. 297, ed. Perez, E., Gonzalez Delgado, R. M., Tenorio-Tagle, G. (Gu03)  
 Held, E. V., de Zeeuw, T., Mould, J., Picard, A., 1992, *AJ*, 103, 851  
 Hernquist, L., 1992, *ApJ*, 400, 460  
 Hernquist, L., Spergel, D. N., Heyl, J. S., 1993, *ApJ*, 416, 415  
 Jerjen, H., 2003, *A&A*, 398, 63  
 Jerjen, H., Binggeli, B., Barazza, F. D., 2004, *AJ*, 127, 771  
 Kawata, D., 1999, *PASJ*, 51, 931  
 Kawata, D., 2001, *ApJ*, 558, 598 (K01)  
 Kormendy, J., 1977, *ApJ*, 218, 333  
 Kroupa, P., 1998, *MNRAS*, 300, 200  
 Marcolini, A., Brighenti, F., D’Ercole, A., 2003, *MNRAS*, 345, 1329  
 Mastropietro, C., Moore, B., Mayer, L., Debattista, V. P., Piffaretti, R., Stadel, J., 2004, submitted to *MNRAS*, astro-ph/0411648  
 Mayer, L., Governato, F., Colpi, M., Moore, B., Quinn, T., Wadsley, J., Stadel, J., Lake, G., 2001, *ApJ*, 559, 754  
 Mayer, L., Moore, B., 2004, *MNRAS*, 354, 477  
 Michaelsen, D., De Rijcke, S., Dejonghe, H., Zeilinger, W. W., Hau, G. K. T., 2003, *ApJ*, 597, L21  
 Michaelsen, D., De Rijcke, S., Zeilinger, W. W., Prugniel, P., Dejonghe, H., Roberts, S., 2004, *MNRAS*, 353, 1293 (M04)  
 Moore, B., Katz, N., Lake, G., Dressler, A., & Oemler Jr., A., 1996, *Nature*, 379, 613  
 Moore, B., Lake, G., Katz, N., 1998, *ApJ*, 495, 139  
 Nagashima, M. & Yoshii, Y., 2004, *ApJ*, 610, 23 (NY04)  
 Nieto, J.-L., Bender, R., Davoust, E., Prugniel, P., 1990, *A&A*, 230, L17  
 Peterson, R. & Caldwell, N., 1993, *AJ*, 105, 1411 (PC93)  
 Press, W. H., Teutolsky, S. A., Vetterling, W. T., Flannery, B. P., 1992, *Numerical recipes in C*, Cambridge University Press, New York, US  
 Schlegel, D. J., Finkbeiner, D. P., & Davis, M., 1998, *ApJ*, 500, 525

Saglia, R. P., Maraston, C., Thomas, D., Bender, R., Colless, M., 2002,  
ApJ, 579, L13

Saito, M., 1979, PASJ, 31, 181

Somerville, R. S., Primack, J. R., Faber, S. M., 2001, MNRAS, 320,  
504

Somerville, R. S., Moustakas, L. A., Mobasher, B., Gardner, J. P.,  
Cimatti, A., Conselice, C., Daddi, E., Dahlen, T., Dickinson, M.,  
Eisenhardt, P., Lotz, J., Papovich, C., Renzini, A., Stern, D., 2004,  
ApJ, 600, 135

Tonry, J. L., Dressler, A., Blakeslee, J. P., Ajhar, E. A., Fletcher, A.  
B., Luppino, G. A., Metzger, M. R., Moore, C. B., 2001, ApJ,  
546, 681

Trujillo, I., Burkert, A., Bell, E. F., 2004, ApJ, 600, L39

van der Marel, R. P.; Franx, M., 1993, ApJ, 407, 525

van Zee, L., Skillman, E. D., Haynes, M. P., 2004, AJ, 128, 121 (vZ04)

Yoshii, Y. & Arimoto, N., 1987, A&A, 188, 13 (YA87)